

Topological charge-2 triply degenerate point: Theory and high-throughput material screeningZining Hu, Lei Jin,^{*} Chenyao Li, Ying Liu, Xuefang Dai, Xiaoming Zhang,[†] and Guodong Liu[‡]*State Key Laboratory of Reliability and Intelligence of Electrical Equipment, and School of Materials Science and Engineering, Hebei University of Technology, Tianjin 300130, China*

(Received 20 November 2023; revised 3 June 2024; accepted 3 July 2024; published 22 July 2024)

The charge-2 (C2) triple point (TP) is a zero-dimensional threefold band degeneracy with a topological charge $|C| = 2$. Different from other types of TP, the C2 TP is expected to have novel physical properties because of its nonzero topological charge. However, the C2 TP is only found in nonmagnetic materials and has not been found in realistic magnetic materials. In this work, we systematically study such fermions in nonmagnetic and ferromagnetic systems. Based on 230 space groups (SGs), we confirm that 13 SGs could host the C2 TP at high-symmetry points. By first-principles calculations and high-throughput material screening, we identify 82 candidate materials, which host a nonmagnetic or ferromagnetic C2 TP. The lattice parameters, magnetic ground states, spin-polarization ratio, and positions of the C2 TP in momentum/energy space of these candidate materials are also given in detail. To support our theory, we take BaPbP₂ and MnBi₁₂O₂₀ as examples for detailed analysis, which host spinless and full spin-polarized C2 TPs. In particular, a long Fermi arc extended in the whole Brillouin zone is clearly observed. Our work paves the way to study the C2 TP and provides candidate materials for future study of physical properties, experimental research, and device application.

DOI: [10.1103/PhysRevB.110.035152](https://doi.org/10.1103/PhysRevB.110.035152)**I. INTRODUCTION**

Topological electronic materials have been developed for more than ten years and play an important role in condensed-matter physics and materials science. Topological insulators were first proposed and realized, and then were extended to topological semimetals with further research. A fundamental of topological semimetal is band crossings, which exhibit particularly rich types. Several works have accomplished a list of complete classification of band crossings in all magnetic space groups and magnetic layer groups [1–5]. According to the degeneracy of the crossing point, topological semimetal can host twofold-, threefold-, fourfold-degeneracy points, etc. Among them, the twofold- and fourfold-degeneracy points are the extensively studied Weyl and Dirac points, upon which are exerted strict constraints by Poincaré symmetry in high-energy physics. In contrast, the triple point (TP) has a relaxed constraint imposed by crystallographic symmetry and exhibits many novel physical properties including unexpected helical anomalies, large negative magnetoresistance, exotic Fermi arc surface states, and unconventional quantum Hall effects [6–9].

Triple points can be classified into the common triple point (CTP), the quadratic triple point (QTP), the quadratic contact triple point (QCTP), and the charge-2 (C2) TP, according to the location of the TP and the band energy dispersion [1]. As shown in Fig. 1(a), the CTP is formed by a linear crossing between a doubly degenerate band and a singly degenerate band, which does not have a well-defined topological charge.

It features a linear energy splitting in any direction in momentum space and can occur on a high-symmetry line or at a high-symmetry point in the Brillouin zone (BZ). As shown in Fig. 1(b), the QTP, like the CTP, is also formed by a linear crossing between a doubly degenerate band and a singly degenerate band and does not have a well-defined topological charge. The difference is that the QTP only occurs along a certain high-symmetry line and has quadratic energy splitting in the plane perpendicular to the high-symmetry line. As shown in Fig. 1(c), the QCTP features a quadratic energy splitting in any direction in momentum space and splits into a doubly degenerate band and a nondegenerate band along a certain high-symmetry line and three nondegenerate bands at generic momentum points. The QCTP only occurs at a high-symmetry point in spinless systems, possessing topological charge $C = 0$.

The C2 TP is different from the three above types of TP in that it carries a defined nonzero topological charge ($|C| = 2$). As shown in Fig. 1(d), it features a linear energy splitting in any direction in momentum space and the C2 TP only occurs at a high-symmetry point in the BZ. As is well known, many peculiar physical phenomena produced in topological semimetals have a great relationship with their topological charge. For example, it may affect the number of topological Fermi arc surface states [10,11], the quantization rate of the quantified circular photocurrent [12–14], and the number of chiral Landau levels associated with the magnetic transport phenomenon and chiral anomaly [15]. The C2 TP also could exhibit striking effects, for instance, super Klein tunneling [16], supercollimation [17], and super Andreev reflection [18,19]. Although the C2 TP is expected to show new topological phenomena, transport behaviors, and spectroscopic responses, it is only found in nonmagnetic materials

^{*}Contact author: jinlei994@163.com[†]Contact author: zhangxiaoming87@hebut.edu.cn[‡]Contact author: gdliu1978@126.com

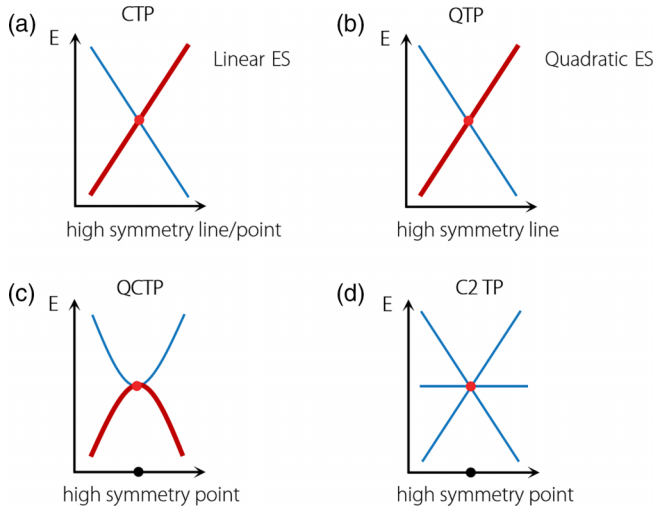


FIG. 1. Schematic figures of the band structure for the (a) CTP, (b) QTP, (c) QCTP, and (d) C2 TP. The bold red line represents the doubly degenerate band and the blue line represents the singly degenerate band. Linear ES represents that the CTP has linear energy splitting in any direction. Quadratic ES represents that the QTP has quadratic energy splitting in the plane normal to the high-symmetry line.

including CoSi [20], RhSi [21], and Mg₃Ru₂ [15] but not yet in magnetic materials.

In this work, we do a systematic theoretical analysis and material screening to identify C2 TP in nonmagnetic (NM) and ferromagnetic (FM) systems. We search all over single-valued 230 space groups (SGs) via symmetry analysis and first-principles calculation, finding 13 SGs and 82 materials that host C2 TP. We also list the basic information of these candidate materials, including the lattice parameters, magnetic ground states, the spin-polarization ratio, and the positions of C2 TPs in momentum/energy space. This screening not only includes complete NM candidate materials with C2 TPs, but also finds such fermions in FM materials. Moreover, we provide NM BaPpT and the half-metal MnBi₁₂O₂₀ as examples to support our discoveries. Our work lays a foundation for the study of physical properties, experimental research, and application of C2 TP in the future.

II. COMPUTATIONAL METHODS

We use the Vienna *ab initio* simulation package for the first-principles calculations, which is based on density functional theory [22,23]. The generalized gradient approximation (GGA) of the Perdew-Burke-Ernzerhof functional is adopted for the exchange-correlation potential [24]. The interaction between electrons and ions is modeled using the projector augmented wave method [25]. The cutoff energy is set as 500 eV. The BZ is sampled by Monkhorst-Pack k mesh with a size of $11 \times 11 \times 11$. During lattice optimization, energy and force convergence criteria are set to 10^{-7} eV and 0.01 eV/Å, respectively. We apply the GGA+ U method to account for the Coulomb interaction of transition-metal elements and rare-earth elements. Among them, the results for BaPpT and MnBi₁₂O₂₀ in the present work are obtained when the U

TABLE I. List of SGs hosting C2 TPs.

SG	BZ	Position	PG	IRRs
195	Γ_c	Γ, R	T	R_4
196	Γ_c^f	Γ	T	R_4
197	Γ_c^v	H, Γ, P	T	R_4
198	Γ_c	Γ	T	R_4
199	Γ_c^v	Γ, H	T	$R_4(\Gamma), R_8(H)$
207, 208	Γ_c	Γ, R	O	R_4 or R_5
209, 210	Γ_c^f	Γ	O	R_4 or R_5
211	Γ_c^v	H, Γ, P	O	R_4 or $R_5(\Gamma, H), R_4(P)$
212, 213	Γ_c	Γ	O	R_4 or R_5
214	Γ_c^v	Γ, H	O	R_4 or $R_5(\Gamma), R_9$ or $R_{10}(H)$

values of Pt and Mn are set to 3 and 4 eV, respectively. We also test different Hubbard U values for 14 materials to determine their features near the Fermi surface in the Supplemental Material [26], including BaPpT and MnBi₁₂O₂₀. The results indicate that these materials always exhibit a C2 TP in a certain range of U values. The surface state is calculated using the WANNIERTOOLS package, based on the maximally localized Wannier functions [27–30]. The irreducible representations of bands are calculated by the IRVSP package [31].

III. SYMMETRY ANALYSIS

Unlike Weyl points, a C2 TP requires additional crystalline symmetry protection to ensure a stable existence and is only located at high-symmetry points in the BZ. The C2 TP is determined by the dimension of the irreducible representations (IRRs) of the little group at high-symmetry points. To study symmetry-protected C2 TPs systematically, we search all three-dimensional (3D) IRRs at high-symmetry points of 230 SGs, unveiling SGs 195–199 and 207–214 that could host this point at high-symmetry points. The minimum point group (PG) at the high-symmetry points protecting the C2 TPs is T , which is a subgroup of O . We also search generators of the little group that determine C2 TPs at high-symmetry points and construct matrix representations of generators. The above symmetry information is summarized in Table I; based on this information, we could construct the $k \cdot p$ Hamiltonian expanded around the C2 TP.

Here we choose the minimum PG T , which is generated by three generators: twofold rotation in the z direction (C_{2z}), twofold rotation in the y direction (C_{2y}), and threefold rotation in the [111] direction ($C_{3,111}$). There exists a 3D IRR R_4 at the Γ point to enable the C2 TP. The three bases are chosen as $\{x, y, z\}$ and the symmetry operators have $M(R)$, where R runs over all generating elements of PG T :

$$M(C_{2z}) = \begin{bmatrix} -1 & 0 & 0 \\ 0 & -1 & 0 \\ 0 & 0 & 1 \end{bmatrix}, \quad M(C_{2y}) = \begin{bmatrix} -1 & 0 & 0 \\ 0 & 1 & 0 \\ 0 & 0 & -1 \end{bmatrix},$$

$$M(C_{3,111}) = \begin{bmatrix} 0 & 1 & 0 \\ 0 & 0 & 1 \\ 1 & 0 & 0 \end{bmatrix}. \quad (1)$$

The Hamiltonian \mathcal{H} should be invariant under the symmetry transformations, namely,

$$M(C_{2z})\mathcal{H}(\mathbf{k})M(C_{2z})^{-1} = \mathcal{H}(-k_x, -k_y, k_z), \quad (2)$$

$$M(C_{2y})\mathcal{H}(\mathbf{k})M(C_{2y})^{-1} = \mathcal{H}(-k_x, k_y, -k_z), \quad (3)$$

$$M(C_{3,111})\mathcal{H}(\mathbf{k})M(C_{3,111})^{-1} = \mathcal{H}(k_z, k_x, k_y). \quad (4)$$

The Hamiltonian takes the form

$$\mathcal{H}_T(\mathbf{k}) = \begin{bmatrix} 0 & (A + iB)k_z & (A - iB)k_y \\ (A - iB)k_z & 0 & (A + iB)k_x \\ (A + iB)k_y & (A - iB)k_x & 0 \end{bmatrix}. \quad (5)$$

IV. MATERIAL REALIZATION

Based on the material database, we go through a series of screening processes in Fig. 2 and finally identify 13 SGs and 82 candidate materials that can have C2 TPs at high-symmetry points. First, for 230 SGs, we use symmetry analysis to determine that SGs 195–199 and 207–214 can possess FM and NM C2 TPs. Based on the Materials Project database, materials in the above SGs are further screened. By determining their magnetic ground states, we obtain 494 NM materials and 225 FM materials. In this process, we also reference the MAGNDATA database and exclude materials that have been experimentally determined to be other magnetic ground states. Then we exclude the insulators by evaluating the band gap and those with metallic band structures (band gap equal to 0 eV) are selected. Because topological surface states come from stable band crossings near the Fermi level, here we choose only the materials with triply degenerate points at $|E - E_F| < 0.5$ eV. Finally, we obtain 82 candidate materials, including 64 NM materials and 18 FM materials. Detailed information about these materials, including their lattice parameters (experimental and optimized), magnetic ground states, spin-polarization ratio, and positions of C2 TPs in momentum/energy space, is summarized in Table II. We also provide magnetic space groups and magnetic point groups of each magnetic material, as shown in Table S2 of the Supplemental Material [26]. In the following, we select two representative C2 TP topological materials (BaPPt and $\text{MnBi}_{12}\text{O}_{20}$) from the screened materials for detailed analysis, and the electronic band structures of the 12 other C2 TP topological materials are shown.

A. Nonmagnetic BaPPt with C2 TP

BaPPt has a cubic crystal belonging to the SG $P2_13$ (No. 198); this material has been synthesized experimentally as early as 1986 [41]. Its lattice structure is shown in Fig. 3(a) and the corresponding BZ is shown in Fig. 3(b). During our computations, the optimized lattice constants of this material are $a = b = c = 6.582 \text{ \AA}$, matching well with the experimental ones ($a = b = c = 6.533 \text{ \AA}$) [41]. In the optimized structure, Ba, P, and Pt atoms occupy the $4a$ (0.139, 0.139, 0.139), $4a$ (0.849, 0.849, 0.849), and $4a$ (0.415, 0.415, 0.415) Wyckoff sites, respectively. We use the optimized lattice structure in the following calculation.

We first discuss the electronic band structure without considering the spin-orbit coupling (SOC). As shown in Fig. 3(c), there is a C2 TP formed by the crossing of three single

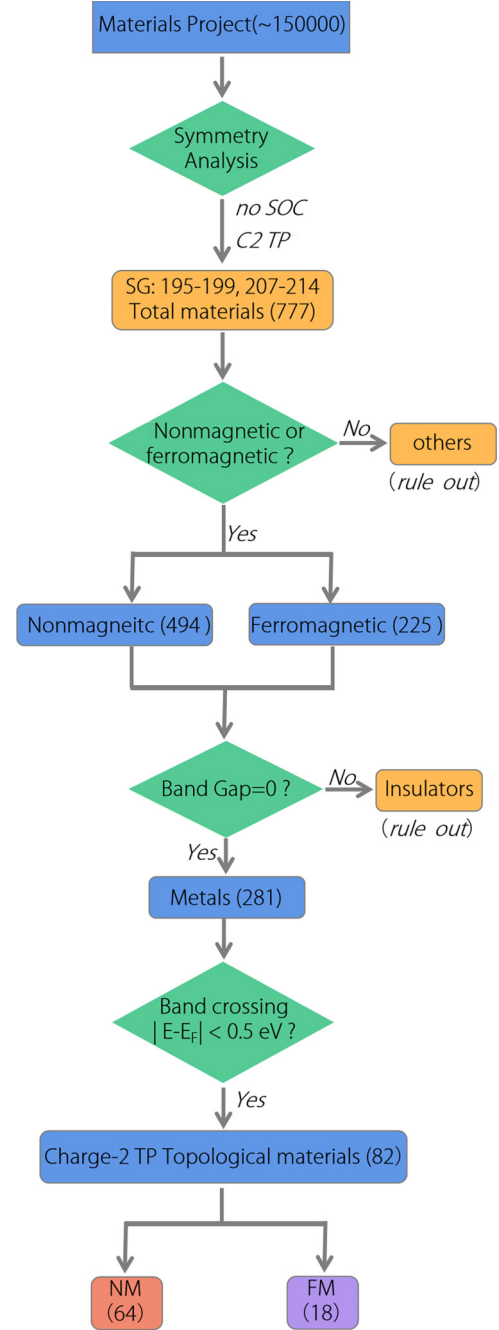


FIG. 2. Flowchart for screening nonmagnetic and ferromagnetic materials with a C2 TP.

bands at the high-symmetry point Γ , located at an energy of -0.077 eV. Further symmetry analysis shows that this triply degenerate band at point Γ is associated with the 3D IRR Γ_4 . There are also two Dirac points (DPs) with topological charge $|C| = 2$ (C2 DPs) near the Fermi level, and both C2 DPs are located at the high-symmetry point R and are very close in energy, one at -0.482 eV and the other at -0.506 eV. At point R , two fourfold-degenerate bands (namely, C2 DPs) carry IRRs $R_1 + R_3$ and $R_2 + R_2$, respectively. A key signature of C2 TPs and C2 DPs is the presence of two Fermi arcs coming from projected images of the bulk band crossing. In Fig. 3(d) we show the projected band spectrum on the (001)

TABLE II. List of material candidates hosting C2 TPs. Also listed are their space group, the locations of the C2 TPs in the BZ, the experimental and optimized lattice constants, the magnetic ground state (MGS), the spin-polarization ratio (SPR), and the energy positions of the C2 TPs.

SG	Location	Material	Lattice (Expt.) (Å)	Lattice (optimized) (Å)	MGS	SPR	Energy (eV)		
195	Γ, R								
196	Γ								
							<i>H</i>	Γ	<i>P</i>
197	H, Γ, P	MnBi ₁₂ O ₂₀	8.838 [32]	8.924	FM [33]	100%	0.108	0.028	0.002
		Bi ₁₂ BO ₂₀		8.786	FM	100%	-0.256	-0.028	-0.027
		LiBi ₁₂ O ₂₀		8.801	NM		-0.197	0.081	0.008
		ZnBi ₁₂ O ₂₀	8.837 [34]	8.832	NM		-0.107	-0.036	-0.218
		YbCd ₆		13.698	NM		-0.146	-0.037	-0.173
		YBi ₁₂ O ₂₀		8.971	NM		-0.304	0.071	-0.183
		HoBi ₁₂ O ₂₀		8.963	NM		-0.298	0.07	-0.179
		ErBi ₁₂ O ₂₀		8.951	NM		-0.314	0.071	-0.179
		YbBi ₁₂ O ₂₀		8.906	NM		-0.276	0.028	-0.144
		DyBi ₁₂ O ₂₀		8.959	NM		-0.322	0.07	-0.185
		BeBi ₁₂ O ₂₀		8.760	NM		-0.271	0.186	-0.048
								Γ	
198	Γ	NiPS	5.538 [35]	5.536	FM	20.3%		-0.327	
		K ₂ Ti ₂ P ₃ O ₁₂	9.869 [36]	10.033	FM	100%		0.002	
		Na ₃ TiP ₃ NO ₉	9.498 [37]	9.630	FM	100%		0.001	
		EuPIr	6.671 [38]	6.272	FM [38]	4.1%		0.419	
		Na ₉ Cu ₂ O ₇		9.903	FM	100%		0.001	
		K ₂ YbSnP ₃ O ₁₂		10.404	NM			-0.043	
		AlPd	4.859 [39]	4.909	NM			-0.418	
		AlAu ₄	6.916 [40]	7.055	NM			0.057	
		BaPPt	6.533 [41]	6.582	NM			-0.077	
		SrSiPd	6.500 [42]	6.570	NM			0.357	
		BeAu	4.668 [43]	4.724	NM			-0.414	
		BiTePd	6.642 [44]	6.757	NM			-0.411	
		GaPt	4.910 [45]	4.973	NM			-0.151	
		BaAsPt	6.716 [41]	6.829	NM			0.025	
		AlPt	4.866 [46]	4.917	NM			-0.166	
		BiPdSe	6.432 [47]	6.537	NM			-0.479	
		CaSiPt	6.320 [48]	6.385	NM			0.367	
		ReSi	4.775 [49]	4.805	NM			0.286	
		SrSiPt	6.485 [42]	6.553	NM			0.420	
		SnRh	5.132 [50]	5.213	NM			-0.062	
		SiTc	4.755 [51]	4.785	NM			0.351	
		GaAg ₉ Se ₆	11.126 [52]	11.322	NM			-0.003	
		SiRh	4.675 [53]	4.729	NM			0.050	
		CoSi	4.438 [54]	4.433	NM			0.035	
		GaPd	4.890 [55]	4.963	NM			-0.412	
		Sr ₈ Al ₇	12.753 [56]	12.762	NM			0.007	
		AlCu ₄	6.260 [57]	6.292	NM			0.143	
		SrAl	12.753 [58]	12.771	NM			-0.099	
		HgPd	5.210 [59]	5.323	NM			-0.022	
		HfSn	5.594 [60]	5.668	NM			-0.079	
		Ag ₄ TeN ₂ O ₆	8.627 [61]	9.535	NM			-0.005	
		Cu ₃ SnAu	6.656 [62]	6.858	NM			-0.070	
		Ag ₄ TeCl ₂ O ₆	8.634 [63]	9.734	NM			-0.032	
		NdSm ₃ Sb ₃		9.432	NM			-0.161	
		SbPtS	6.174 [64]	6.290	NM			-0.396	
		NiSbS	5.910 [65]	5.930	NM			-0.442	
							Γ		<i>H</i>
199	Γ, H	Li ₆ La ₃ Nb ₂ O ₁₂		11.168	FM	100%	-0.007		-0.022
							Γ		<i>H</i>
		UCo	5.504 [66]	5.467	NM		0.232		0.298
		Pd ₃ Pb ₂ S ₂		7.347	NM		-0.258		-0.026

TABLE II. (Continued.)

SG	Location	Material	Lattice (Expt.) (Å)	Lattice (optimized) (Å)	MGS	SPR	Energy (eV)			
							Γ	R		
207, 208	Γ, R	$\text{Na}_{11}\text{U}_5\text{O}_{16}$	9.543 [67]	9.684	FM	100%	-0.028	0.012		
		$\text{Na}_{11}\text{Bi}_5\text{O}_{16}$		9.607	FM	70.9%	-0.120	-0.035		
209, 210 211	Γ H, Γ, P									
212	Γ	$\text{Na}_3\text{Mn}_3\text{O}_8$		8.769	FM	100%	Γ	-0.036		
		$\text{Li}_2\text{TiCr}_3\text{O}_8$		8.398	FM	100%		-0.121		
		LiMn_5O_8		8.523	FM	100%		0.078		
		$\text{Li}_2\text{Cu}_3\text{F}_8$		8.532	FM	100%		0.016		
		$\text{Li}_3\text{Mn}_3\text{O}_8$		8.275	FM	100%		-0.002		
		$\text{Li}_2\text{Ti}_3\text{CrO}_8$		8.442	FM	68.2%		0.125		
		$\text{Li}_2\text{Fe}_3\text{NiO}_8$		8.360	FM	100%		0.001		
		V_8C_7	8.330 [68]	8.335	NM			0.205		
		Li_2BPt_3	6.755 [69]	6.845	NM			-0.020		
		Li_2BPd_3	6.753 [69]	6.834	NM			-0.099		
		$\text{Li}_2\text{Ti}_3\text{NbO}_8$		8.559	NM			0.013		
		213	Γ	Mg_3Ru_2	6.935 [70]	6.965	NM		Γ	-0.108
				$\text{V}_3\text{Zn}_2\text{N}$	6.600 [71]	6.578	NM			-0.038
				$\text{Nb}_3\text{Al}_2\text{C}$	7.070 [71]	7.130	NM			-0.070
$\text{Nb}_3\text{Al}_2\text{N}$	7.030 [71]			7.079	NM			-0.281		
$\text{Mo}_3\text{Pd}_2\text{N}$	6.817 [72]			6.878	NM			-0.241		
$\text{Mo}_3\text{Pt}_2\text{N}$	6.835 [73]			6.902	NM			0.281		
Fe_2Re_3	6.430 [74]			6.413	NM			0.117		
Nb_3Au_2	7.090 [75]			7.137	NM			-0.059		
$\text{Ta}_3\text{Al}_2\text{C}$	7.020 [76]			7.095	NM			-0.129		
$\text{V}_3\text{Ga}_2\text{N}$	6.620 [71]			6.611	NM			0.306		
Mn_2Al_3	6.424 [77]			6.395	NM			0.314		
$\text{Re}_2\text{W}_3\text{C}$	6.872 [78]			6.957	NM			0.142		
$\text{Al}_2\text{Mo}_3\text{C}$	6.866 [79]			6.890	NM			0.239		
V_3Ga_2	6.620 [80]			6.546	NM			-0.069		
214	Γ, H			Gd_3CCl_3	9.295 [81]	9.386	FM	38.5%	Γ	0.114
				La_3SbI_3	12.780 [82]	12.950	NM			0.110
		La_3AsI_3	12.533 [82]	12.660	NM			0.180		
		La_3PI_3	10.762 [83]	10.877	NM			0.190		
		Br_3SiTb_3	9.930 [84]	10.100	NM			0.327		
								H	-0.169	

surface of BaPpT, which clearly reveals two pieces of Fermi arcs (indicated by the white arrows), which is consistent with their topological charge $|C| = 2$. Similar to the C2 TP at the high-symmetry point Γ , the C2 DP at the high-symmetry point R also has two Fermi arcs. As shown in Fig. 3(e), the two white points near each other on the (111) surface are projections of two C2 DPs, and two Fermi arcs emanate from each C2 DP (indicated by the white arrows).

For BaPpT, whose elements are relatively heavy, the SOC is not negligible. Figure 3(d) shows the electronic band structures of BaPpT with SOC. We can observe that the previous C2 TP splits into a twofold-degenerate Weyl point (WP) and a fourfold-degenerate Dirac point (DP). Their IRRs are Γ_5 and $\Gamma_6 + \Gamma_7$, respectively. The previous C2 DP splits into a sextuple point (SP) and a WP. Here both the DP at the Γ point and the SP at the R point possess topological charge $|C| = 4$. At point R , two sextuply degenerate bands (namely, C4 SPs) both carry IRRs $R_7 + R_7$. They carry a large topological charge and

thus also show multiple Fermi arcs. As shown in Fig. 4(b), four Fermi arcs emanating from the DP can be observed from the electronic spectrum of the (001) surface. Analogously, we also observe four Fermi arcs in the electronic spectrum of the (111) surface shown in Fig. 4(c).

B. Half-metal $\text{MnBi}_{12}\text{O}_{20}$ with C2 TP

$\text{MnBi}_{12}\text{O}_{20}$ belongs to the SG $I23$ (No. 197), which can be synthesized in experiment [32]. The crystal structure of this material is shown in Fig. 5(a) and the BZ is shown in Fig. 5(b). During our computations, the optimized lattice constants are $a = b = c = 8.924$ Å, matching well with the experimental ones ($a = b = c = 8.838$ Å) [32]. In the optimized structure, the Bi and Mn atoms are located at the $24f$ (0.193, 0.496, 0.334) and $2a$ (0, 0, 0) Wyckoff sites, respectively. The O atoms occupy the $24f$ (0.620, 0.382, 0.739), $8c$ (0.389, 0.389, 0.389), and $8c$ (0.794, 0.794, 0.794) Wyckoff

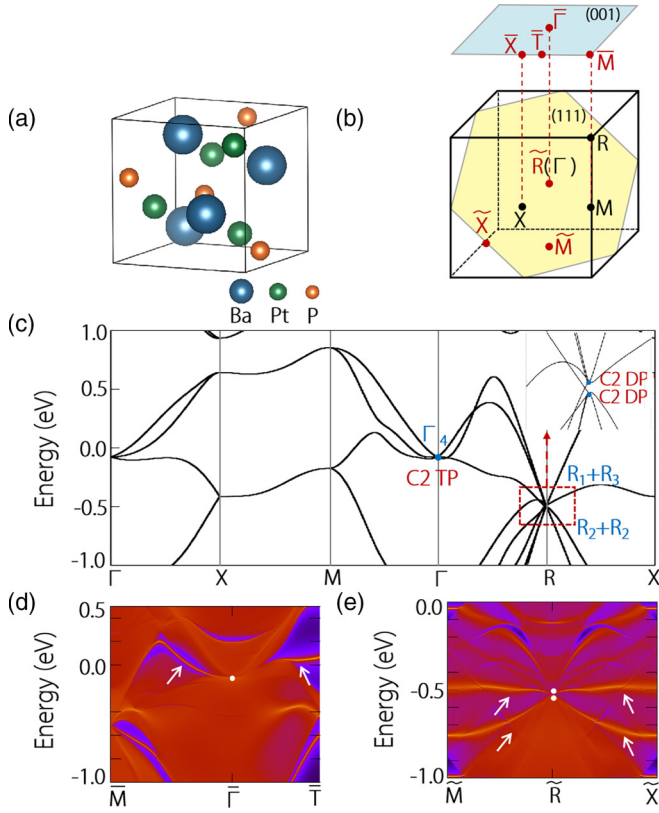


FIG. 3. (a) Crystal structure for BaPtP (SG 198). (b) Bulk (001) and (111) surfaces in the Brillouin zone, with high-symmetry points and projected high-symmetry points. (c) Electronic band structure for BaPtP without SOC. The blue dots indicate the C2 TP at the Γ point and the C2 DP at the R point. (d) Projected spectrum on the (001) surface for BaPtP. The white dot indicates the projection of the C2 TP and the white arrows point to the corresponding Fermi arcs. (e) Projected spectrum on the (111) surface for BaPtP. The white dots indicate the projection of the C2 DP and the white arrows point to the corresponding Fermi arcs.

sites. The optimized lattice structure is used in our calculations.

Before studying the electronic structure, we first determine the magnetic ground state of the material. We take three possible magnetic configurations into consideration, including antiferromagnetic (AFM), FM, and NM states. Consequently, we find that the FM state has the lowest energy compared with NM and AFM states. The results show that the FM state is 4.77 meV lower than the AFM state and 1.3 eV lower than the NM state for one unit cell, confirming that $\text{MnBi}_{12}\text{O}_{20}$ has a FM ground state. In the ground state, $\text{MnBi}_{12}\text{O}_{20}$ has an integer magnetic moment of $3\mu_B$, which almost originates from the transition metal Mn element. The following discussion is based on the FM state.

When SOC is not considered, the band structures of the $\text{MnBi}_{12}\text{O}_{20}$ compound in Figs. 5(c) and 5(d) show two crucial features. First, the spin-up band is metallic with the band through the Fermi level, while the spin-down band is insulating with a 2.5 eV energy gap, indicating that the material is a half-metal, where the fully-spin-polarized conduction electrons can be realized. Second, focusing on the spin-up

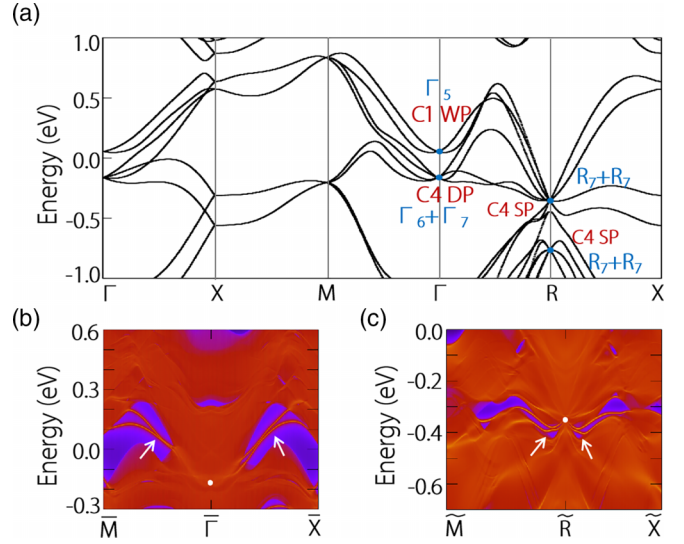


FIG. 4. (a) Electronic band structure of BaPtP with SOC. (b) Projected spectrum on the (001) surface. The white dot indicates the C4 DP and the arrows point to the Fermi arcs. (c) Projected spectrum on the (111) surface. The white dot indicates the C4 SP and the arrows point to the Fermi arcs.

band structure, there are 100% spin-polarized TPs at the high-symmetry points H , Γ , and P and these TPs are very close to the Fermi level without other extraneous bands. Symmetry analysis shows that the bands at the H , Γ , and P points near the Fermi level are triply degenerate bands (namely, C2 TPs), associated with IRRs H_4 , Γ_4 , and P_4 , respectively. Through first-principle calculations and symmetry analysis, we also determine that these TPs have a topological number $|C| = 2$. Most importantly, we found the C2 TP in realistic magnetic materials, which had previously only been observed in non-magnetic materials. Here, not only are all FM materials with a C2 TP screened, but also the $\text{MnBi}_{12}\text{O}_{20}$ compound as an example is discussed in detail.

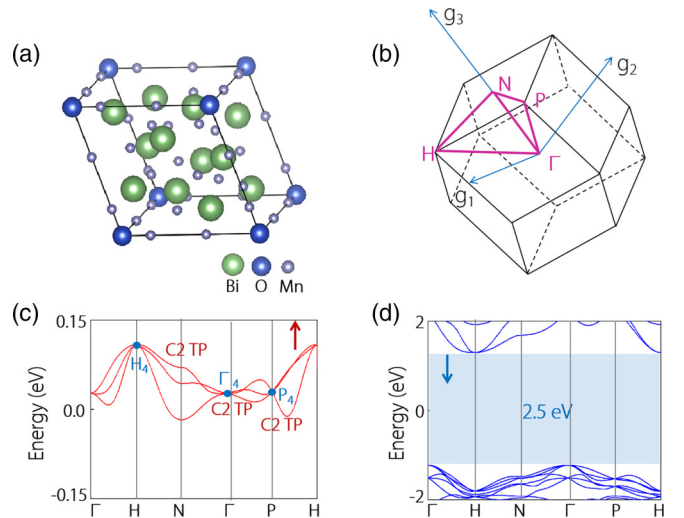


FIG. 5. (a) Crystal structure and (b) Brillouin zone of the $\text{MnBi}_{12}\text{O}_{20}$ compound. (c) Spin-up band structure, showing metallic character. (d) Spin-down band structure, exhibiting insulating character with a band gap of 2.5 eV.

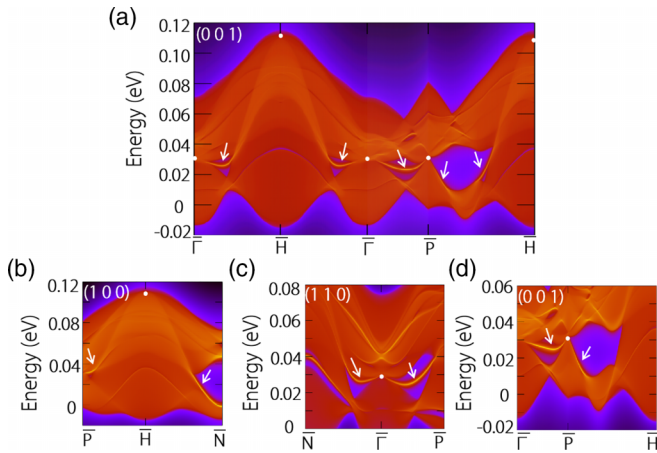


FIG. 6. (a) Projected spectrum on the (001) surface of MnBi₁₂O₂₀. The white dots indicate the positions of the C2 TPs. Two Fermi arcs (indicated by arrows) connect these C2 TPs. Also shown are the surface states of (b) (100) and (c) (110) surfaces. (d) Surface state on the opposite terminating surface of (001).

One of the most representative characteristics of C2 TPs is the Fermi arc surface states. When projecting onto the (001) surface of the MnBi₁₂O₂₀ compound in Fig. 6(a), we can observe that there are two Fermi arcs starting from C2 TPs at the high-symmetry points H , Γ , and P , which are consistent with their topological number $|C| = 2$. Notably, the Fermi arcs of these C2 TPs are connected to each other and thus are extended in the whole BZ. In addition, by projecting onto the (100) and (110) surfaces, we can also clearly observe the Fermi arcs from C2 TPs at the high-symmetry points H and Γ [shown in Figs. 6(b) and 6(c)]. The Fermi arcs of MnBi₁₂O₂₀ spread over the whole BZ and can be clearly observed on multiple projection surfaces, which is very conducive to future observations in experiment.

C. Band structures of other materials with a C2 TP

For the materials in Table II, in addition to the above BaPPT and MnBi₁₂O₂₀ materials, we also select some materials from SGs 198, 199, 212, and 213, including NM and FM materials, and show their band structures in Fig. 7. These materials all

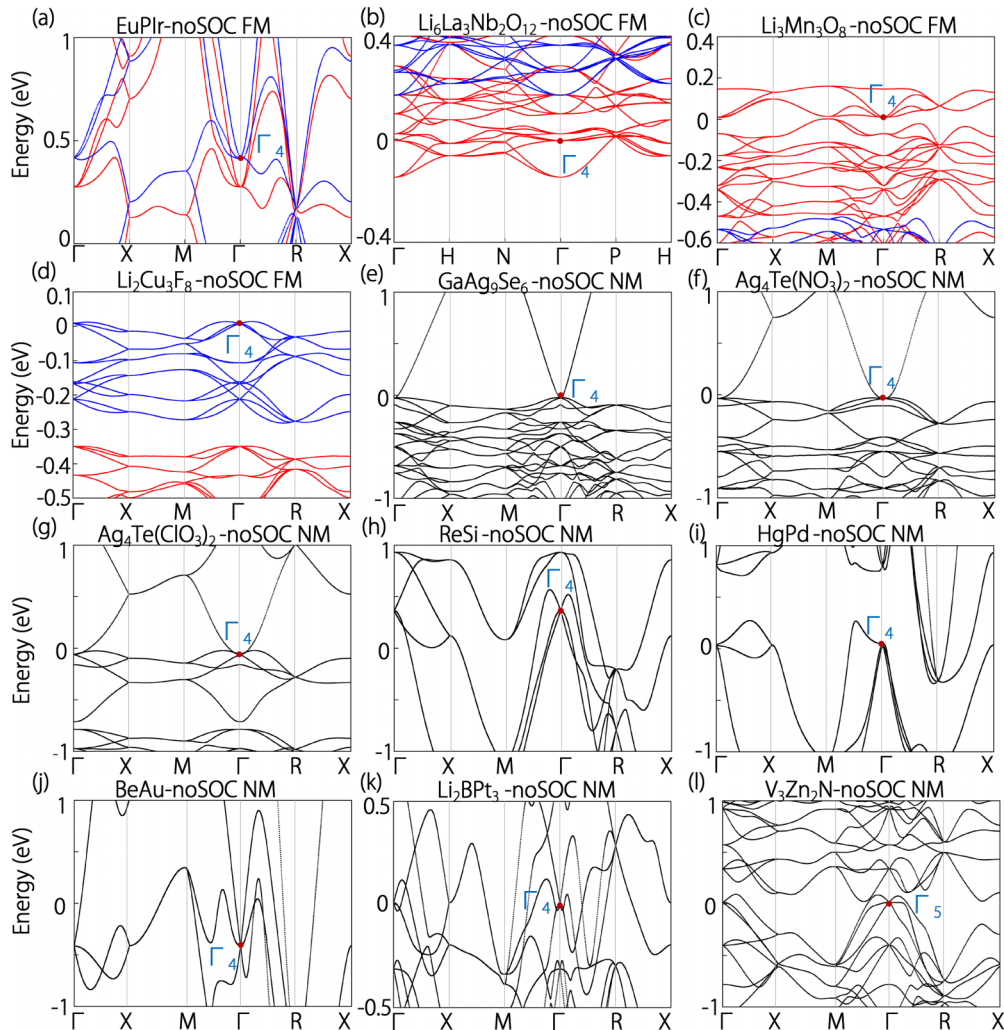


FIG. 7. Electronic band structures of (a) EuPIr, (b) Li₆La₃Nb₂O₁₂, (c) Li₃Mn₃O₈, (d) Li₂Cu₃F₈, (e) GaAg₉Se₆, (f) Ag₄Te(NO₃)₂, (g) Ag₄Te(ClO₃)₂, (h) ReSi, (i) HgPd, (j) BeAu, (k) Li₂BPT₃, and (l) V₃Zn₂N without SOC. The C2 TPs are highlighted by red dots.

have C2 TPs within 0.5 eV, where $\text{Li}_6\text{La}_3\text{Nb}_2\text{O}_{12}$, $\text{Li}_3\text{Mn}_3\text{O}_8$, and $\text{Li}_2\text{Cu}_3\text{F}_8$ have fully-spin-polarized C2 TPs. We also calculate their IRRs of C2 TPs, which are marked in their band structures.

V. CONCLUSION

Before closing, we have several remarks. First, we systematically studied C2 TPs in realistic ferromagnetic materials. Several works [1–4] have thoroughly studied the complete classification of emergent particles in all magnetic space groups based on symmetry analysis and modeling and have given the basic information of these emergent particles, including the symmetry conditions, the effective Hamiltonian, the band dispersion, and the topological characters. Tang and Wan [2], and Xu *et al.* [5] also predicted hundreds of topological magnetic materials. Although these works thoroughly investigated topological magnetic materials based on the theoretical model and analysis, the exploration and investigation of specific C2 TPs in realistic materials was still inadequate, especially in ferromagnetic materials with a high spin-polarized ratio. Therefore, it is important to investigate ferromagnetic materials with C2 TPs. Most of the materials mentioned in this work are realistic materials and are reported to be C2 TP materials. Incidentally, we reported nonmagnetic TPs in a previous work [15] that included the classification of TPs and material realization in nonmagnetic systems. For screened nonmagnetic C2 TP materials, this work is more complete than that due to the updating of the Materials Project database.

Second, we systematically screened all realistic ferromagnetic and nonmagnetic materials that host C2 TPs and provided much basic information, including space group number, point group, high-symmetry points hosting C2 TPs, lattice parameters (experimental and optimized), magnetic ground states, energy positions of C2 TP, and IRRs. We also calculated the spin-polarization ratio for all ferromagnetic materials and found 13 realistic materials that host fully-spin-polarized C2 TP.

Third, all screened candidate materials have C2 TPs in the region $|E - E_F| < 0.5$ eV, which is promising for detection in experiments. Topologically protected metal states on material

surfaces originate from stable band crossings near the Fermi level. The C2 TP must be close to Fermi level, because in this case, low-energy electrons and most solid properties can exhibit the characteristics of such a band crossing point. The energy band near the Fermi level should be clean enough, and there are no other unrelated energy bands; otherwise the experimental results cannot fully reflect the nature of the C2 TP. Therefore, exploring ideal realistic materials that host C2 TP is necessary.

Fourth, there are some additional properties in concrete materials with C2 TPs. For example, the material $\text{MnBi}_{12}\text{O}_{20}$ has fully-spin-polarized C2 TPs at three high-symmetry points near the Fermi level and their Fermi arcs are connected to each other, forming a long Fermi arc extending into the whole Brillouin zone, which greatly facilitates experimental observations.

In summary, by symmetry analysis and first-principles calculations, we identified 13 SGs from 230 SGs where C2 TPs can exist at high-symmetry points, and through a screening process, we high-throughput screened 82 candidate materials, including NM and FM materials. In order to be as detailed as possible, we listed much basic information about all candidate materials. We used NM BaPpt and half-metal $\text{MnBi}_{12}\text{O}_{20}$ as examples and discussed their band structures, C2 TP characteristics, and topological surface states in detail. Finally, we also showed band structures of 12 other materials with C2 TPs. Our work provides a rich data set of C2 TPs in NM and FM materials, paving the way for observation in future experiments.

ACKNOWLEDGMENTS

This work was supported by the Postdoctoral Fellowship Program of CPSF (Grant No. GZC20230662), the Hebei Natural Science Foundation (S&T Program of Hebei, Grant No. A2023202032), the 2024 Hebei Province Higher Education Institutions Scientific Research Project (Grant No. JZX2024023), the Overseas Scientists Sponsorship Program of Hebei Province (Grant No. C20230502), and the 333 Talent Project of Hebei Province (Grant No. A20231001).

-
- [1] Z.-M. Yu, Z. Zhang, G.-B. Liu, W. Wu, X.-P. Li, R.-W. Zhang, S. A. Yang, and Y. Yao, *Sci. Bull.* **67**, 375 (2022).
 - [2] F. Tang and X. Wan, *Phys. Rev. B* **105**, 155156 (2022).
 - [3] G.-B. Liu, Z. Zhang, Z.-M. Yu, S. A. Yang, and Y. Yao, *Phys. Rev. B* **105**, 085117 (2022).
 - [4] Z. Zhang, G.-B. Liu, Z.-M. Yu, S. A. Yang, and Y. Yao, *Phys. Rev. B* **105**, 104426 (2022).
 - [5] Y. Xu, L. Elcoro, Z.-D. Song, B. J. Wieder, M. Vergniory, N. Regnault, Y. Chen, C. Felser, and B. A. Bernevig, *Nature (London)* **586**, 702 (2020).
 - [6] Z. Zhu, G. W. Winkler, Q. S. Wu, J. Li, and A. A. Soluyanov, *Phys. Rev. X* **6**, 031003 (2016).
 - [7] H. Weng, C. Fang, Z. Fang, and X. Dai, *Phys. Rev. B* **93**, 241202(R) (2016).
 - [8] J. B. He, D. Chen, W. L. Zhu, S. Zhang, L. X. Zhao, Z. A. Ren, and G. F. Chen, *Phys. Rev. B* **95**, 195165 (2017).
 - [9] Y. Xu and L.-M. Duan, *Phys. Rev. B* **96**, 155301 (2017).
 - [10] X. Wan, A. M. Turner, A. Vishwanath, and S. Y. Savrasov, *Phys. Rev. B* **83**, 205101 (2011).
 - [11] A. A. Burkov, M. D. Hook, and L. Balents, *Phys. Rev. B* **84**, 235126 (2011).
 - [12] F. de Juan, A. G. Grushin, T. Morimoto, and J. E. Moore, *Nat. Commun.* **8**, 15995 (2017).
 - [13] F. Flicker, F. de Juan, B. Bradlyn, T. Morimoto, M. G. Vergniory, and A. G. Grushin, *Phys. Rev. B* **98**, 155145 (2018).
 - [14] F. de Juan, Y. Zhang, T. Morimoto, Y. Sun, J. E. Moore, and A. G. Grushin, *Phys. Rev. Res.* **2**, 012017(R) (2020).
 - [15] L. Tian, Y. Liu, W.-W. Yu, X. Zhang, and G. Liu, *Phys. Rev. B* **104**, 045137 (2021).
 - [16] R. Shen, L. B. Shao, B. Wang, and D. Y. Xing, *Phys. Rev. B* **81**, 041410(R) (2010).
 - [17] A. Fang, Z. Q. Zhang, S. G. Louie, and C. T. Chan, *Phys. Rev. B* **93**, 035422 (2016).

- [18] X. Feng, Y. Liu, Z.-M. Yu, Z. Ma, L. K. Ang, Y. S. Ang, and S. A. Yang, *Phys. Rev. B* **101**, 235417 (2020).
- [19] X. Feng, W. Wu, Y. Huang, Z.-M. Yu, and S. A. Yang, *Phys. Rev. B* **104**, 115116 (2021).
- [20] P. Tang, Q. Zhou, and S.-C. Zhang, *Phys. Rev. Lett.* **119**, 206402 (2017).
- [21] G. Chang, S.-Y. Xu, B. J. Wieder, D. S. Sanchez, S.-M. Huang, I. Belopolski, T.-R. Chang, S. Zhang, A. Bansil, H. Lin *et al.*, *Phys. Rev. Lett.* **119**, 206401 (2017).
- [22] G. Kresse and J. Hafner, *Phys. Rev. B* **49**, 14251 (1994).
- [23] G. Kresse and J. Furthmüller, *Phys. Rev. B* **54**, 11169 (1996).
- [24] J. P. Perdew, K. Burke, and M. Ernzerhof, *Phys. Rev. Lett.* **77**, 3865 (1996).
- [25] P. E. Blöchl, *Phys. Rev. B* **50**, 17953 (1994).
- [26] See Supplemental Material at <http://link.aps.org/supplemental/10.1103/PhysRevB.110.035152> for the band structures of 14 materials at different Hubbard U values, and the magnetic space groups and magnetic point groups of magnetic materials.
- [27] N. Marzari and D. Vanderbilt, *Phys. Rev. B* **56**, 12847 (1997).
- [28] I. Souza, N. Marzari, and D. Vanderbilt, *Phys. Rev. B* **65**, 035109 (2001).
- [29] M. L. Sancho, J. L. Sancho, J. L. Sancho, and J. Rubio, *J. Phys. F* **15**, 851 (1985).
- [30] Q. Wu, S. Zhang, H.-F. Song, M. Troyer, and A. A. Soluyanov, *Comput. Phys. Commun.* **224**, 405 (2018).
- [31] J. Gao, Q. Wu, C. Persson, and Z. Wang, *Comput. Phys. Commun.* **261**, 107760 (2021).
- [32] U. Delicat, S. Radaev, M. Trömel, P. Behrens, Y. F. Kargin, and A. Mar'in, *J. Solid State Chem.* **110**, 66 (1994).
- [33] L. A. S. de Oliveira, A. Pentón-Madrigal, A. Guimarães, and J. Sinnecker, *J. Magn. Magn. Mater.* **401**, 890 (2016).
- [34] S. Kirik, V. Kutvitskii, and T. Koryagina, *Zh. Strukt. Khim.* **26**, 90 (1985).
- [35] A. J. Foecker and W. Jeitschko, *J. Solid State Chem.* **162**, 69 (2001).
- [36] A. Leclaire, A. Benmoussa, M. Borel, A. Grandin, and B. Raveau, *J. Solid State Chem.* **78**, 227 (1989).
- [37] I. V. Zatonovskiy, T. V. Vorobjova, K. V. Domasevitch, I. V. Ogorodnyk, and N. S. Slobodyanik, *Acta Cryst. E* **62**, i32 (2006).
- [38] C. Lux, A. Mewis, S. Junk, A. Gruetz, and G. Michels, *J. Alloys Compd.* **200**, 135 (1993).
- [39] M. Zurkirch, M. DeCrescenzi, M. Erbudak, and A. R. Kortan, *Phys. Rev. B* **56**, 10651 (1997).
- [40] H. Büchler and K.-J. Range, *J. Less-Common Met.* **161**, 347 (1990).
- [41] G. Wenski and A. Mewis, *Z. Anorg. Allg. Chem.* **535**, 110 (1986).
- [42] J. Evers and G. Oehlinger, *J. Solid State Chem.* **62**, 133 (1986).
- [43] B. Cullity, *Trans. Am. Inst. Min. Metall. Eng.* **171**, 396 (1947).
- [44] J. D. Childs and S. R. Hall, *Can. Mineral.* **12**, 61 (1973).
- [45] M. Bhargava, A. Gadalla, and K. Schubert, *J. Less-Common Met.* **42**, 69 (1975).
- [46] P. Eßlinger and K. Schubert, *Int. J. Mater. Res.* **48**, 126 (1957).
- [47] B. Joshi, A. Thamizhavel, and S. Ramakrishnan, *J. Phys.: Conf. Ser.* **592**, 012069 (2015).
- [48] J. Evers, G. Oehlinger, K. Polborn, and B. Sendlinger, *J. Solid State Chem.* **103**, 45 (1993).
- [49] R. A. McNees, Jr. and A. W. Searcy, *J. Am. Chem. Soc.* **77**, 5290 (1955).
- [50] K. Schubert, *Z. Naturforsch. A* **2**, 120 (1947).
- [51] J. B. Darby, Jr., J. Downey, and L. Norton, *J. Less-Common Met.* **8**, 15 (1965).
- [52] J. P. Deloume, R. Faure, H. Loiseleur, and M. Roubin, *Acta Cryst. B* **34**, 3189 (1978).
- [53] K. Göransson, I. Engström, and B. Nörling, *J. Alloys Compd.* **219**, 107 (1995).
- [54] P. Demchenko, J. Kończyk, O. Bodak, R. Matvijishyn, L. Muratova, and B. Marciniak, *Chem. Met. Alloys* **1**, 50 (2008).
- [55] M. Armbrüster, H. Borrmann, M. Wedel, Y. Prots, R. Giedigkeit, and P. Gille, *Z. Krist. New Cryst. Struct.* **225**, 617 (2010).
- [56] G. Bruzzone and F. Merlo, *J. Less-Common Met.* **39**, 1 (1975).
- [57] J. L. Leach, *J. Inst. Met.* **92**, 93 (1964).
- [58] M. Fornasini and F. Merlo, *Acta Cryst. B* **32**, 1864 (1976).
- [59] H. Bittner and H. Nowotny, *Monatsh. Chem.* **83**, 287 (1952).
- [60] O. Schob and E. Parthé, *Acta Cryst.* **17**, 452 (1964).
- [61] E. Schultze-Rhönhof and G. Bergerhoff, *Acta Cryst. B* **25**, 2645 (1969).
- [62] O. Karlsen, A. Kjekshus, and E. Rost, *Acta Chem. Scand.* **44**, 197 (1990).
- [63] E. Schultze-Rhönhof, *Acta Cryst. B* **28**, 1969 (1972).
- [64] F. Hulliger, *Nature (London)* **198**, 382 (1963).
- [65] L. S. Ramsdell, *Am. Mineral.* **10**, 281 (1925).
- [66] W. K. Noyce and A. H. Daane, *The uranium-cobalt system*, U.S. Atomic Energy Commission Report No. AECD-2826, 1946.
- [67] S. Bartram and R. Fryxell, *J. Inorg. Nucl. Chem.* **32**, 3701 (1970).
- [68] D. Rafaja, W. Lengauer, P. Ettmayer, and V. Lipatnikov, *J. Alloys Compd.* **269**, 60 (1998).
- [69] U. Eibenstein and W. Jung, *J. Solid State Chem.* **133**, 21 (1997).
- [70] R. Pöttgen, V. Hlukhyy, A. Baranov, and Y. Grin, *Inorg. Chem.* **47**, 6051 (2008).
- [71] W. Jeitschko, H. Nowotny, and F. Benesovsky, *Monatsh. Chem.* **95**, 1212 (1964).
- [72] A. El-Himri, F. Sapiña, R. Ibañez, and A. Beltrán, *J. Mater. Chem.* **11**, 2311 (2001).
- [73] A. El-Himri, D. Marrero-López, and P. Núñez, *J. Solid State Chem.* **177**, 3219 (2004).
- [74] Y. Kuzma and P. Kripyakevich, *Sov. Phys. Cryst.* **10**, 466 (1966).
- [75] V. Antonov, E. Bokhenkov, B. Dorner, V. Fedotov, G. Grosse, A. Latynin, F. Wagner, and R. Wordel, *J. Alloys Compd.* **264**, 1 (1998).
- [76] J. Eitzkorn, M. Ade, and H. Hillebrecht, *Inorg. Chem.* **46**, 1410 (2007).
- [77] W. Köster and E. Wachtel, *Int. J. Mater. Res.* **51**, 271 (1960).
- [78] A. Lawson, *J. Less-Common Met.* **23**, 103 (1971).
- [79] W. Jeitschko, H. Nowotny, and F. Benesovsky, *Monatsh. Chem.* **94**, 247 (1963).
- [80] H.-G. Meißner and K. Schubert, *Int. J. Mater. Res.* **56**, 475 (1965).
- [81] E. Warkentin and A. Simon, *Rev. Chim. Miner.* **20**, 488 (1983).
- [82] C. Zheng, O. Oeckler, H. Mattausch, and A. Simon, *Z. Anorg. Allg. Chem.* **627**, 2151 (2001).
- [83] P. K. Dorhout, M. W. Payne, and J. D. Corbett, *Inorg. Chem.* **30**, 4960 (1991).
- [84] H. Mattausch, O. Oeckler, and A. Simon, *Z. Kristallogr.* **217**, 459 (2002).